The Interaction of Methanol, Acetone, and Acetaldehyde with Ice and Nitric Acid-Doped Ice: Implications for Cirrus Clouds

Paula K. Hudson, Mark A. Zondlo, and Margaret A. Tolbert*

Department of Chemistry and Biochemistry and the Cooperative Institute for Research in Environmental Sciences, University of Colorado, Boulder 80309

Received: July 16, 2001; In Final Form: October 3, 2001

The uptake of methanol, acetone, and acetaldehyde by ice and nitric acid/ice surfaces representative of cirrus clouds has been measured using a Knudsen cell flow reactor equipped with FTIR spectroscopic observation of the condensed phase. Sticking coefficients and total equilibrium coverage for the organics on ice were obtained over the temperature range of 120−200 K. Both the sticking coefficients and coverage were found to decrease with increasing temperature for all three species. The coverage data was fit using a Langmuir adsorption model, and the results were extrapolated to typical cirrus cloud temperatures. By the use of estimates for the gaseous concentrations of the organic species, calculated coverages on ice at 210 K are extrapolated to be on the order of 10^{10} molecules/cm^2 (10^{-4} ML) for methanol and acetone and $<5 \times 10^9$ molecules/cm^2 ($<10^{-5}$ ML) for acetaldehyde. Such small coverages constitute an insignificant portion of each gas-phase species being lost to cirrus clouds. Additionally, the surface coverages of $\leq 10^{-4}$ monolayers (ML) are likely to be too small to impact heterogeneous chemistry. Uptake of methanol, acetone, and acetaldehyde was also studied on several forms of nitric acid-coated ice at temperatures from 190 to 200 K. Studies on nitric acid trihydrate (NAT) and ice with monolayer coverage of HNO_3 showed no measurable uptake in the examined temperature range for all three species. While no uptake was observed on a supercooled HNO_3/H_2O solution for acetone or acetaldehyde at $T = 200$ K, this solution did show enhanced uptake of methanol at 200 K relative to pure ice.

Introduction

Our understanding of the chemistry of the upper troposphere has undergone significant revisions in recent years. One of the most dramatic examples of this is the recognition of the important role that oxygenated hydrocarbons play in this part of the atmosphere. Species such as methanol (CH_3OH), acetone ($(CH_3)_2C(O)$), and acetaldehyde (CH_3CHO) are abundant in the upper troposphere, with measured mixing ratios of 400−900 pptv, 300−3000 pptv, and 30−100 pptv, respectively.[1−4] Their destruction is dominated by reaction with OH and photolysis, while their sources include direct biogenic emissions and biomass burning.

The destruction of oxygenated hydrocarbons results in the formation of HO_x ($HO_x = OH + HO_2$). The OH radical is responsible for most of the chemistry in the troposphere. Thus, understanding the sources and sinks for OH is vital to assessing the future oxidative capacity of our atmosphere. For most of the troposphere, ozone photolysis in the presence of water vapor is the major source of HO_x:

$$O_3 + h\nu \rightarrow O(^1D) + O_2 \ (\lambda < 310 \text{ nm}) \qquad (1)$$

$$O(^1D) + H_2O \rightarrow 2\ OH \qquad (2)$$

However, in the upper troposphere, the mixing ratio of water is sufficiently low to make this mechanism inefficient. It has recently been recognized that HO_x production from oxygenated hydrocarbons is important, providing as much HO_x as reactions 1 and 2 in some regions of the atmosphere.[1] Calculations have shown that the oxidation of acetaldehyde and methanol in biomass burning plumes leads to a net production of 0.8 HO_x (i.e., one molecule of organic produces 0.8 molecules of HO_x) and the oxidation of acetone creates a net source of 3.6 HO_x.[5] Furthermore, recent modeling studies suggest that acetone photooxidation provides a global source of HO_x to the upper troposphere while the presence of aldehydes and other oxygenated hydrocarbons enhances HO_x locally in the tropics.[6]

In addition to having a major impact on the HO_x cycle, oxygenated hydrocarbons may influence NO_y ($NO_y = NO_x + N_2O_5 + HNO_3 + ClONO_2 + PAN + ...$) in the troposphere by reactions of their decomposition products or by direct reactions with NO_y species. For example, one decomposition product of acetone, the peroxyacetyl radical ($CH_3C(O)O_2$), can react with NO_2 to form peroxyacetyl nitrate (PAN):

$$CH_3C(O)O_2 + NO_2 + M \rightarrow PAN + M \qquad (3)$$

PAN is of great atmospheric interest due to its role in transporting NO_x ($NO_x = NO + NO_2$) to rural areas where it can contribute to smog formation.

Direct heterogeneous reactions involving oxygenated hydrocarbons and NO_y species could be important in converting HNO_3 into NO_x. Atmospheric models consistently overpredict the HNO_3/NO_x ratio by factors of 2−10.[7−9] One previous attempt to reconcile this imbalance relied on reaction of formaldehyde with HNO_3 on tropospheric aerosols or clouds according to[10]

$$HCHO + HNO_3 \rightarrow HONO + HCOOH \qquad (4)$$

While laboratory studies have shown that this reaction does occur on sulfuric acid surfaces,[11,12] the rate appears to be too

10.1021/jp012718m CCC: $22.00
Published on Web 03/06/2002

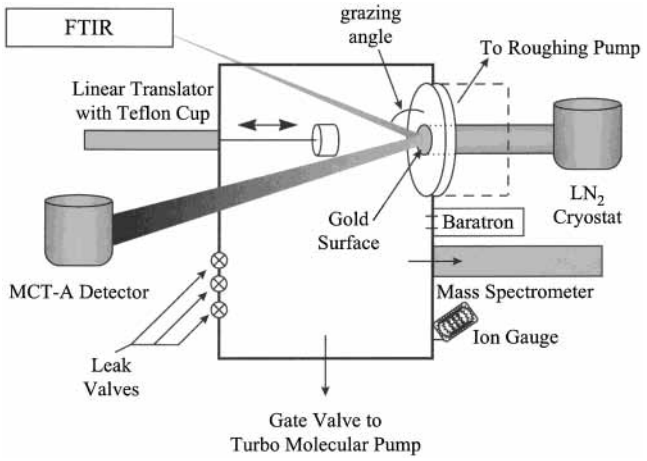

Figure 1. Experimental setup showing the Knudsen cell flow reactor and FTIR−RAS.

slow to completely solve the HNO_3/NO_x dilemma.[13] It is possible that heterogeneous reactions of other oxygenated organic species such as methanol, acetone, and acetaldehyde may help alleviate this problem.

Although the abundance and importance of oxygenated hydrocarbons in the upper troposphere are now recognized, a complete understanding of their sources and sinks is still lacking. For example, a recent study reports that methanol sources are more than twice as large as known sinks.[2] It further states that methanol was found to be less abundant in the upper troposphere relative to acetone implying unknown, possibly heterogeneous sinks for methanol.[2] A recent study has proposed that the heterogeneous conversion of methanol to formaldehyde on cirrus could be an additional sink for methanol.[14] Further measurements in the Pacific show values of acetone and acetaldehyde 2−10 times larger, respectively, than models can predict.[4] To help develop a more complete understanding of the budgets of methanol, acetone, and acetaldehyde in the upper troposphere, we have examined possible heterogeneous loss of these species on various thin films representative of upper tropospheric cirrus clouds.

Cirrus clouds cover as much as 30% of the Earth's surface at any given time.[15] Although mainly composed of ice, these clouds may have a significant coverage of adsorbed HNO_3.[16,17] To explore these conditions, we have examined the interaction of methanol, acetone, and acetaldehyde with pure ice and ice coated with a monolayer of nitric acid. To further understand these interactions, we also studied these species on pure NAT surfaces and supercooled HNO_3/H_2O solutions.

Experimental Section

The experimental setup, shown schematically in Figure 1, combines a Knudsen cell flow reactor and Fourier transform infrared reflection absorption spectroscopy (FTIR−RAS) to simultaneously monitor gas and condensed phases, respectively.[18,19] The apparatus consists of a single stainless steel chamber that houses a vertically mounted gold substrate upon which thin films are deposited. Two potassium chloride, KCl, windows are located on either side of the chamber for passage of the IR beam. Chamber pressures are monitored using an ionization gauge and absolute capacitance manometer, while gas-phase constituents are analyzed by an electron-impact quadrupole mass spectrometer. Partial pressures of the organic species are determined by calibrating the mass spectrometer signals to the ion gauge and absolute capacitance manometer. Because each species is calibrated as the sole component of the chamber, we are able to get a direct calibration between the mass spectrometer and the absolute pressure. Water partial pressures are read directly using the absolute capacitance manometer. Three leak valves are used for the introduction of water, nitric acid, and either methanol, acetone, or acetaldehyde. A gate valve separates the chamber from a turbomolecular pump. The gate valve contains a 0.17 cm^2 orifice (A_h) for the determination of accurate molecular flows during an experiment when the gate valve is closed.[20] A Teflon cup with a volume of 7 cm^3 with an O-ring seal is located on a pneumatic linear translator across from the gold surface. When the translator is extended completely, the Teflon cup covers the gold surface, isolating it from the rest of the chamber.

The optically flat gold surface ($d = 2.54$ cm) is cooled by thermal contact with a liquid nitrogen-filled cryostat and resistively heated to a desired temperature (120−200 K) using a Minco heater controlled by a Eurotherm temperature programmer. The substrate temperature is measured using three type T (copper−constantan) thermocouples mounted to the back of the gold surface using a thermally conductive epoxy. Temperature gradients across the surface are less than 0.5 K. The heating/cooling assembly is housed in a differentially pumped stainless steel sleeve with a Teflon seal between the sleeve and gold substrate. In this setup, the gold substrate is the only cold surface in the chamber.

In a typical experiment, the gold surface is first cooled to the desired temperature. A flow of water or nitric acid/water is introduced into the chamber and a thin film of either ice or nitric acid/ice is deposited. The growth and stability of the film is monitored by FTIR−RAS. Under some temperature conditions, a constant flow of H_2O or HNO_3/H_2O is necessary to keep a constant film thickness for the duration of the experiment.

Once a stable film at equilibrium with the vapor has been attained, the Teflon cup is extended over the film, isolating it from the chamber. Independent tests have shown that the film maintains a constant composition and thickness while isolated. A flow of the organic species is then introduced into the chamber and monitored using the mass spectrometer to ensure a steady flow. Once a steady flow of organic has been established, the Teflon cup is retracted, exposing the film to the organic. If the organic is adsorbed to the film, there is a decrease in the mass spectrometer signal. Retraction of the Teflon cup results in an extremely small volume change, <0.05% of the chamber volume. Therefore, any decrease in signal is the result of loss to the surface and not from dilution due to volume expansion or to wall loss. If uptake is self-limited, the signal subsequently recovers to its original level after the steady-state coverage has been attained. If the organic condenses directly onto the film, the signal remains at its lowest value until the surface is again isolated from the organic. Once the surface has been isolated, the mass spectrometer signal returns to its original level.

Surface coverages are calculated by first converting the mass spectrometer signal of each organic species to an absolute pressure by using the calibration to the absolute capacitance manometer. Errors in pressure are less than 10%. Calculations of steady-state flow rates of the organic are determined by using the Knudsen effusion relation:

$$F = \frac{PA_h}{(2\pi mkT)^{0.5}} \tag{5}$$

where P is the partial pressure of organic, A_h is the effective area of the gate valve orifice (0.17 cm^2), m is the molecular

weight of the organic species, and T is the temperature of the gas phase defined as room temperature. When the surface is exposed and uptake occurs, the partial pressure is lower and thus the flow out of the chamber is lower. Once an equilibrium coverage of organic on the film is established, the steady-state flow of molecules returns to its original signal because the additional loss to the surface is no longer present. The number of molecules lost from the gas phase is simply the integrated area of the loss and recovery of the flow signals as a function of time. The surface coverage (molecules/cm^2) of the species is attained by dividing the number of molecules lost from the gas phase by the geometric surface area of the ice, which is assumed to be that of the gold substrate, $A_s = 5.07$ cm^2. At the temperatures used in this experiment, smooth films, as determined spectroscopically, could be deposited. Recent studies on the roughness of ice films vapor-deposited at different temperatures have shown that using the geometric surface area of the substrate is a close approximation to the ice film surface area below 160 K.[21] If the surface area of the ice film were greater than that of the gold substrate, the calculated coverage would be smaller than reported. The atmospheric significance of this will be addressed later. In experiments in which condensation of the organic occurs (i.e., no recovery of the signal), coverages are not calculated. Uptake is unlimited, and therefore, coverage is dependent on exposure. For this reason, this paper only contains data with submonolayer coverages obtained in experiments at temperatures greater than the condensation temperature.

The initial sticking coefficient, γ_o, can be obtained from the initial drop in the mass spectrometer signal:

$$\gamma_o = \frac{A_h}{A_s}\left(\frac{F_o - F}{F}\right) \tag{6}$$

where F_o is the initial flow of organic molecules through the chamber and F is the value after exposure to the film. Because of the negligible volume change with retraction of the Teflon cup, the entire drop in the mass spectrometer signal is attributed to uptake onto the film. This allows for measurements of sticking coefficients up to a value of $\gamma_o = 0.3$.

Results and Discussion

Preparation and Characterization of Ice Films. To begin an experiment, we first ensure that we have the appropriate film of interest using FTIR−RAS to determine film composition. Figure 2 shows typical infrared spectra for the films used in this study. The spectrum of an ice film at 200 K is shown in panel a and illustrates the characteristic OH stretch from ~3500−3000 cm^{-1} and the ice libration near 850 cm^{-1}. Similar spectra were obtained at all temperatures examined. Film stability at all temperatures is determined by monitoring the integrated area of the OH stretching region. A typical film, approximately 50 nm thick,[22] is considered stable when the integrated area under the OH stretching region changes by less than 0.5% over 100 sec. This translates to less than a 1 nm change in film thickness over 100 sec. At temperatures above 165 K, a constant flow of water vapor, equivalent to the water vapor determined by Marti and Mauersberger,[23] must be established to maintain a constant film thickness during the experiment. Between 150 and 165 K, the background water in the chamber is comparable to the vapor pressure of the ice film. Below 150 K, the calculated water vapor pressure significantly drops off.[23] However, our spectroscopic data support little or no growth or evaporation of films at all temperatures.

Previous studies using this chamber have examined the type of HNO_3/H_2O films that form when pure ice is exposed to HNO_3 vapor under various temperature and pressure conditions.[16,20,24] The spectra in Figure 2b,c,d are similar to previously observed results and can therefore be considered representative spectra. Figure 2b shows a typical spectrum of an ice film with monolayer (ML) HNO_3 coverage. To achieve this film, an ice film at $T = 200$ K is exposed to pressures of $HNO_3 \leq 1 \times 10^{-6}$ Torr until the growth of the NO_3^- asymmetric stretches are just barely discernible in the IR around 1435 and 1350 cm^{-1}. Prolonged exposure of the film to these low pressures of HNO_3 does not result in any further changes. Figure 2c shows a supercooled HNO_3/H_2O solution. To form a supercooled HNO_3/H_2O solution, extended exposure of HNO_3 to the ice film at $T = 200$ K at higher HNO_3 pressures is required. The conversion into the supercooled solution is denoted by an increase in the two NO_3^- peaks at 1435 and 1350 cm^{-1} and a rounding or smoothing out of the OH stretching region from 3500 to 3000 cm^{-1} as well as the loss of the ice libration at 850 cm^{-1}. Figure 2d shows a NAT film. NAT growth is accomplished one of two ways. In the first, an ice film is deposited at 190 K. Once a constant film thickness is established, the ice is exposed to HNO_3 forming a supercooled solution. With small decreases in H_2O pressure, NAT crystallizes out of solution as evidenced by the two NO_3^- peaks combining to one peak around 1395 cm^{-1}, a sharp NO_3^- peak at 820 cm^{-1}, and a sharp peak around 3425 cm^{-1} in the H_2O region indicating a crystalline solid. The second way of forming NAT involves first depositing an ice film at 175 K. Exposure of ice to HNO_3 at this low-temperature results in immediate NAT crystallization. The NAT film temperature is then increased to 190 K. No changes in reactivity were noted upon varying the NAT film preparation technique.

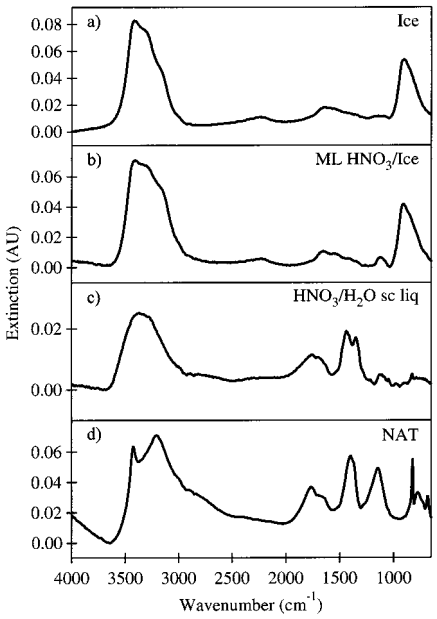

Figure 2. Reference FTIR−RAS spectra of (a) ice, (b) ice with monolayer HNO_3 coverage, (c) supercooled HNO_3/H_2O solution, and (d) NAT.

Uptake of Methanol, Acetone, and Acetaldehyde on Ice. The uptake of methanol, acetone, and acetaldehyde on ice at atmospherically relevant temperatures, $T > 200$ K, was below our limit of detection of 10^{12} molecules/cm^2. Therefore, experiments were performed at lower temperatures at which significant uptake was observed. Figure 3 shows typical uptake curves for methanol on ice at $T = 180$, 167.5, and 160 K. A constant flow of methanol, 1.6×10^{13} molecules/sec ($P \approx 2.7 \times 10^{-7}$ Torr), was established prior to $t = 450$ s. At $t = 450$ s, the Teflon cup was retracted exposing the ice film to the methanol. All three

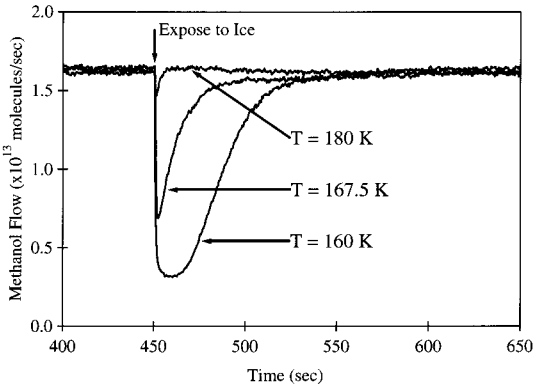

Figure 3. Mass spectrometer signal calibrated to methanol flow upon exposure of ice film to methanol at temperature noted.

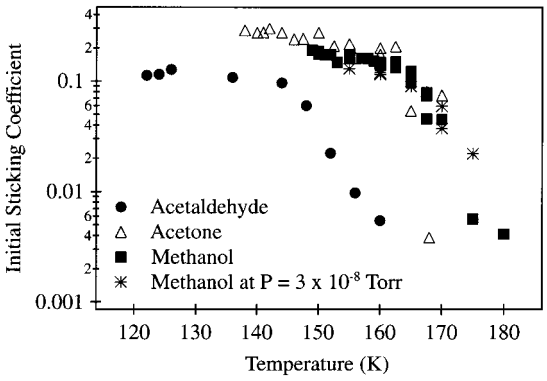

Figure 4. Sticking coefficients for methanol (■ and ∗), acetone (△), and acetaldehyde (●) as a function of ice film temperature.

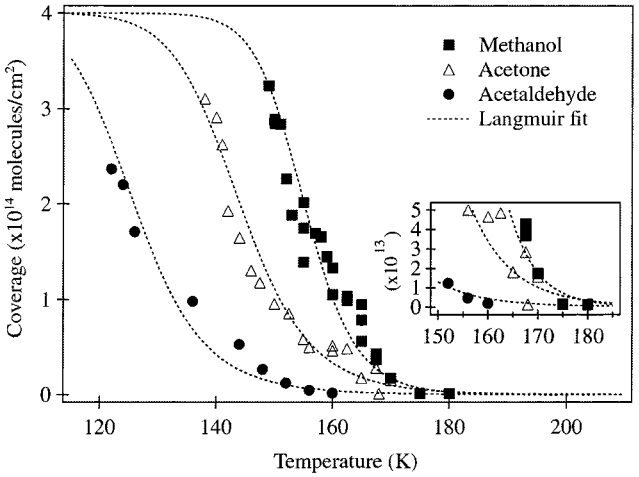

Figure 5. Coverage uptake curves for methanol (■), acetone (△), and acetaldehyde (●) as a function of ice film temperature. The dashed lines are Langmuir best fits.

experiments show a significant drop in methanol signal upon exposure to the ice film. The initial sticking coefficient (γ_o) is determined using the magnitude of this initial drop and eq 6. Calculated sticking coefficients for these three experiments are $\gamma_o = 0.004$, 0.046, and 0.138 for temperatures of 180, 167.5, and 160 K, respectively.

After the initial drop, all signals "saturate", that is, they recover to their original level. While each of these films was isolated from the methanol at different times, there was no change in signal upon isolation with any of them. The recovery of the mass spectrometer signal, or saturation of the surface with methanol, also supports the stability of our films. If the films were growing, a steady increase in the uptake of methanol would occur. The recovery time until saturation varies with the temperature of the ice film with the coldest experiment having the longest recovery time. The area of the loss and recovery of the methanol signal is used to calculate the number of molecules lost from the gas phase and, in turn, the coverage of methanol on the ice film. Therefore, the largest coverage occurs at the coldest temperatures, and the smallest coverage occurs at the warmest temperatures. At temperatures less that $T = 149$ K, condensation of methanol on the ice film occurs. This appears as a drop in the signal with no recovery. While submonolayer coverages of methanol on ice are below the detection limit of the FTIR−RAS, the condensation of multilayers of methanol on the ice is observed in the IR.

Uptake curves similar to methanol were obtained for acetone ($P_{\text{acetone}} = 3.1 \times 10^{-7}$ Torr) and acetaldehyde ($P_{\text{acetaldehyde}} = 3.0 \times 10^{-7}$ Torr). The initial sticking coefficient results for methanol (solid squares and asterisks), acetone (open triangles), and acetaldehyde (solid circles) as a function of ice film temperature are shown in Figure 4. For all three species, the sticking coefficient decreases with increasing temperature. The sticking coefficients for methanol and acetone are quite similar with values for methanol ranging from 0.2 at 150 K to 4×10^{-3} at 180 K. Acetone sticking coefficients overlap those of methanol at temperatures greater than 150 K; however, below 150 K the sticking coefficient continues to rise to our measurement limit of $\gamma_o = 0.3$. Acetaldehyde sticking coefficients are much lower than either methanol or acetone ones with values ranging from 0.12 at 120 K to 5×10^{-3} at 160 K.

The decrease in initial sticking coefficient with increasing temperature could be due to an observation of a net process incorporating both adsorbing molecules to the surface and desorbing molecules from the surface. During the 1−2 s that it takes to reach the minimum value, a significant coverage of the organic could be developing on the ice if the true initial sticking coefficient was unity. While this may be a factor for both acetone and acetaldehyde, we feel the decrease in sticking coefficient with increasing temperature for methanol is real. We have obtained sticking coefficients for methanol using pressures ranging from $P_{\text{methanol}} = 3.0 \times 10^{-8}$ to 3×10^{-7} Torr. As seen in Figure 4, little variation is observed between the sticking coefficients at $P_{\text{methanol}} = 3 \times 10^{-8}$ Torr (asterisks) and those, represented by the solid squares, at $P_{\text{methanol}} = 3 \times 10^{-7}$ Torr. These measurements span an order of magnitude in methanol pressure and are in good agreement with each other. If the decrease in γ_o with temperature was due to competition between adsorption and desorption, one would expect to see a decrease in γ_o using higher pressures. Therefore, we believe our measurements of the initial sticking coefficient for methanol do indeed show a decrease in value as temperature increases. However, because we do not have the pressure-dependent data for acetone and acetaldehyde, we cannot rule out the possibility of measuring a net uptake as temperature increases for these species.

The same experiments used for calculating sticking coefficients are also used to determine equilibrium coverage. The saturated coverage results for methanol (solid squares), acetone (open triangles), and acetaldehyde (solid circles) experiments as a function of ice film temperature are shown in Figure 5. Similar to the trend in sticking coefficients, coverage increases with decreasing temperature. At the lowest temperatures, multilayers for all species grow before a complete monolayer is deposited. The maximum monolayer coverage (Θ_{max}) is calculated using the liquid density (ρ) at 293 K, and the molecular weight (MW), to approximate the radius for each

TABLE 1: Summary of Boiling and Melting Points, Solubility, and Temperature Required for a Coverage of 1×10^{14} molecules/cm^2 on Ice for Each Species

	boiling point[a] (°C)	melting point[a] (°C)	solubility (M/atm)	temperature to reach 1×10^{14} molecules/cm^2 on ice[d] (K)
methanol	65	−93.9	220[b]	160
acetone	56.2	−95.4	30[b]	151
acetaldehyde	20.8	−121	13[c]	133

[a] Handbook of Chemistry and Physics, 73rd edition.[28] [b] Scientific Assessment of Stratospheric Ozone, 1989.[29] [c] Gaffney and Senum.[30] [d] This study.

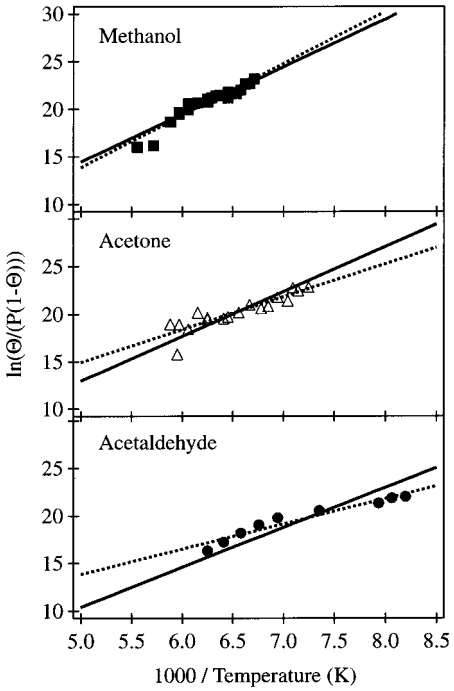

Figure 6. Plots for methanol, acetone, and acetaldehyde to determine ΔH°_{ads} and ΔS°_{ads} using eq 10. The dashed lines are least-squares fits to the data. The solid lines are determined by setting the intercept at −10.57 (corresponding to $\Delta S^{\circ}_{ads} = -21$ cal/(mol K)) with a least-squares fit to the data to determine slope.

molecule as if it were a sphere ($^4/_3\pi r^3 = MW/(\rho N_A)$). The calculated radius of the molecule is then used to approximate the maximum monolayer surface coverage ($\Theta_{max} = 1/(\pi r^2)$). Using this method, we find an average $\Theta_{max} = 4 \times 10^{14}$ molecules/cm^2 for all three species. Therefore, the maximum coverage reported is that of the largest submonolayer coverage obtained, before multilayer growth begins. Measured methanol coverages range from $\sim 3 \times 10^{14}$ molecules/cm^2 at 150 K to our lower limit of detection of 10^{12} molecules/cm^2 at 180 K. Acetone coverage is similar, but its maximum coverage shifts to a lower temperature, ~140 K. Although the sticking coefficients of methanol and acetone are similar, the overall coverage of acetone is lower than that of methanol at the same temperature. That is to say, initially methanol and acetone stick to the surface equally, however, the final equilibrium coverage of acetone is less than that of methanol. Acetaldehyde maximum coverage is at a much lower temperature starting at 120 K. Thus, the temperature required to reach a given coverage decreases from methanol to acetone to acetaldehyde. This trend in uptake follows trends in melting point, boiling point, and solubility in water at 25 °C, as displayed in Table 1.

TABLE 2: Summary of ΔH°_{ads} and ΔS°_{ads} for Each Species

	from best fit to data		assuming Trouton's rule	
	ΔH°_{ads} (kcal/mol)	ΔS°_{ads} (cal/(mol K))	ΔH°_{ads} (kcal/mol)	ΔS°_{ads} (cal/(mol K))
methanol	−10.8	−26.8	−9.9	−21
acetone	−6.8	−4.6	−9.4	−21
acetaldehyde	−5.3	1.1	−8.3	−21

Because the coverages for these organics on ice at atmospherically relevant temperatures are below our detection limit, we have attempted to model the observed uptake and extrapolate to higher temperatures. We use a Langmuir model to fit our experimental data. Briefly, the Langmuir model assumes an equilibrium between gas- and adsorbed-phase species:

$$\text{organic(g)} \overset{K}{\leftrightarrow} \text{organic(ad)} \tag{7}$$

Under these conditions, fractional surface coverage (Θ/Θ_{max}) is given by

$$\frac{\Theta}{\Theta_{max}} = \frac{KP_A}{1 + (KP_A)} \tag{8}$$

where P_A is the pressure of the organic species referenced to STP (1 atm) and Θ_{max} is the maximum monolayer coverage on the surface. The equilibrium constant, K, is given by thermodynamics to be

$$K = \exp\left(\frac{-(\Delta H^{\circ}_{ads} - T\Delta S^{\circ}_{ads})}{RT}\right) \tag{9}$$

where ΔH°_{ads} and ΔS°_{ads} are the standard enthalpy and entropy of adsorption, respectively. Rearranging eqs 8 and 9 results in

$$\ln\left\{\frac{\frac{\Theta}{\Theta_{max}}}{P_A\left(1 - \frac{\Theta}{\Theta_{max}}\right)}\right\} = \frac{-(\Delta H^{\circ}_{ads} - T\Delta S^{\circ}_{ads})}{RT} \tag{10}$$

In our experiment, Θ and P are experimentally measured. The data, in the form of eq 10, is plotted in Figure 6. Again, P_A is the standard-state pressure of the organic species (referenced to STP) and the Θ/Θ_{max} is the standard-state coverage assuming Θ_{max} is one full monolayer of coverage. The dashed line in this figure has been determined by a least-squares linear fit to the data. The slope of this line yields $\Delta H^{\circ}_{ads}/R$. The entropy, ΔS°_{ads}, was obtained from the intercept ($\Delta S^{\circ}_{ads}/R$). The values determined for ΔH°_{ads} and ΔS°_{ads} are shown in Table 2. As discussed further below, all of the ΔH°_{ads} values are reasonable. However, the ΔS°_{ads} values obtained from this technique seem spuriously high for acetone and acetaldehyde. A great deal of uncertainty exists within the entropy values because of the magnitude of the extrapolation required. Therefore, a second analysis has been applied to the data where ΔS°_{ads} was set to be −21 cal/(mol K) according to Trouton's rule. ΔH°_{ads} was then redetermined by a least-squares fit to the data. These data are shown as a solid line in Figure 6 and are also included in Table 2.

Other techniques have been used to determine enthalpies and entropies of organic species interacting with other surfaces. In particular, the uptake of methanol by liquid water droplets as well as on liquid water surfaces has been studied.[25,26] The process of accommodation of a vapor into liquid droplets or

adsorption onto a liquid surface is different from adsorption onto a solid surface. However, the values obtained for methanol are quite comparable. For example, Jayne et al. experimentally determined $\Delta H_{methanol} = -8.0$ kcal/mol and $\Delta S_{methanol} = -34.9$ cal/(mol K) for the accommodation of methanol vapor by water droplets.[25] Donaldson and Anderson experimentally determined $\Delta H_{methanol} = -9.4$ kcal/mol and $\Delta S_{methanol} = -11.9$ cal/(mol K) for accommodation of methanol vapor onto a water surface.[26] The values for $\Delta H_{methanol}$ are in close agreement with both results. Our determined $\Delta S_{methanol}$ falls between the two referenced values, but again, there is a great deal of uncertainty in this calculation. Donaldson and Anderson also examined acetone adsorption onto the water surface.[26] Their values of $\Delta H_{acetone}$ and $\Delta S_{acetone}$, -12.0 kcal/mol and -22.5 cal/(mol K), respectively, are quite different from our values. However, when fixing our $\Delta S_{acetone}$ to -21 cal/(mol K), our value for ΔH^{o}_{ads} is in much better agreement with Donaldson and Anderson with a value of -9.4 kcal/mol. By examining the values of ΔS^{o}_{ads} obtained for both methanol from Jayne et al. ($\Delta S_{methanol} = -34.9$ cal/(mol K)) and methanol and acetone from Donaldson and Anderson ($\Delta S_{methanol} = -11.9$ cal/(mol K), $\Delta S_{acetone} = -22.5$ cal/(mol K)), the use of Trouton's rule is a fairly good assumption.

The Langmuir best fits to the coverage data on a linear scale are shown as the dashed curve in Figure 5. While the Langmuir fits model the data quite well, they tend to overpredict the coverages at the higher temperatures for all three species, as shown in the inset in Figure 5. We can obtain upper limits to the experimental coverages on cirrus clouds by extrapolating the fits to 210 K and assuming atmospherically relevant pressures of 2.0×10^{-7} Torr, 7.9×10^{-8} Torr, and 1.8×10^{-8} Torr for methanol, acetone, and acetaldehyde, respectively. These extrapolations predict coverages of 3.0×10^{10} molecules/cm^2 (7.5×10^{-5} ML) for methanol, 5.6×10^{10} molecules/cm^2 (1.4×10^{-4} ML) for acetone, and 5.2×10^{9} molecules/cm^2 (1.3×10^{-5} ML) for acetaldehyde.

Uptake of Methanol, Acetone, and Acetaldehyde on HNO_3/Ice. Figure 7 shows the calibrated mass spectrometer signal, flow, for methanol exposed to (a) ice, (b) an ice film with 1 ML HNO_3 coverage, (c) a supercooled 4:1 HNO_3/H_2O solution, and (d) a NAT film. All films are at 200 K with the exception of the NAT film, which is at 190 K. After a constant film thickness is established for each film, the Teflon cup is extended, isolating the film from the chamber. Methanol, at a flow rate of approximately 1.6×10^{13} molecules/(cm^2 s) (2.7×10^{-7} Torr), is introduced into the chamber, and a steady flow is established. At $t = 1100$ s, the Teflon cup is retracted from the surface exposing the film to the methanol. The methanol flow does not change when exposed to the film in Figure 7, part a, b, or d. The supercooled HNO_3/H_2O solution shows a small uptake on the order of 4×10^{12} molecules/cm^2, evidenced by the small drop and subsequent recovery of the methanol flow, $\gamma_o = 0.003$. At $t = 1200$ s, the Teflon cup is again extended, covering the film. No change in the methanol flow is observed for any of the films upon isolation. For the case of the supercooled HNO_3/H_2O solution, the constant signal indicates the complete saturation of the methanol uptake prior to isolation of the film. Similar experiments were conducted for acetone and acetaldehyde on ice, 1 ML HNO_3 coverage, supercooled HNO_3/H_2O, and NAT. However, for acetone and acetaldehyde, no uptake was observed at 200 K on any of these surfaces.

The enhanced uptake for methanol on the supercooled solution at 200 K most likely results because adsorption onto the surface of a liquid is more efficient than uptake onto a crystalline solid. Results of increased reactivity on liquid surfaces have been observed with similar systems.[27] Additionally, the uptake may not be limited to only the surface. Diffusion into the liquid, as opposed to diffusion into the crystalline solid, may also be an enhanced process.

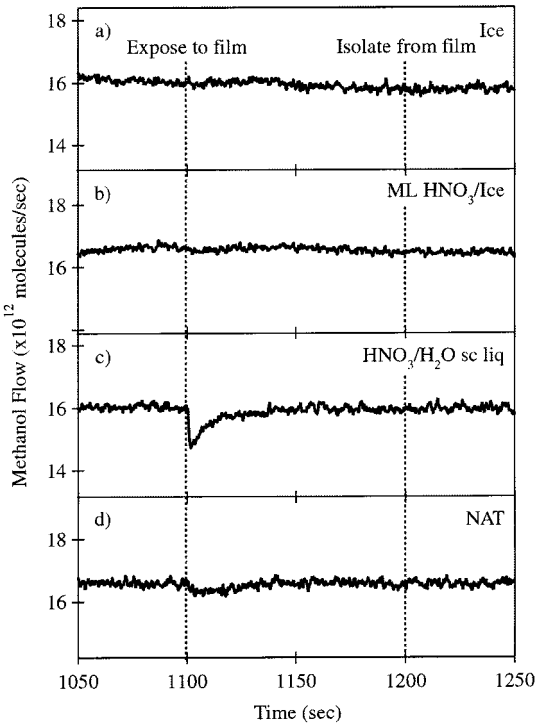

Figure 7. Mass spectrometer signal calibrated to methanol flow upon exposure of (a) ice at $T = 200$ K, (b) ice with monolayer HNO_3 coverage at $T = 200$ K, (c) supercooled HNO_3/H_2O solution at $T = 200$ K, and (d) NAT at $T = 190$ K to methanol.

No gas-phase reaction products were observed with the reactions of any of the species on ice or nitric acid/ice films. Condensed phase products may have formed; however, coverages were below our limits of detection.

Atmospheric Implications

The data collected here can be used to estimate surface coverages for methanol, acetone, and acetaldehyde on ice clouds in the upper troposphere. Extrapolation of the Langmuir fits to 210 K predicts coverages of 3.0×10^{10} molecules/cm^2 (7.5×10^{-5} ML) for methanol, 5.6×10^{10} molecules/cm^2 (1.4×10^{-4} ML) for acetone, and 5.2×10^{9} molecules/cm^2 (1.3×10^{-5} ML) for acetaldehyde. For all three species, the presence of HNO_3 on the ice surface, when it remains in a crystalline form, does not enhance the uptake at atmospherically relevant temperatures. Zondlo et al. showed that under conditions of high HNO_3 partial pressures, addition of HNO_3 to an ice film results in a supercooled solution. With the formation of a supercooled HNO_3/H_2O solution, the uptake of methanol increases at $T = 200$ K. However, even with this enhanced uptake, the expected coverage remains on the order of 10^{12} molecules/cm^2 (3.8×10^{-2} ML) at 200 K and does not represent a large surface coverage. If the surface area of the ice film were in fact larger than the geometric surface area of the gold substrate, the coverage of all three species would decrease. In any case, the coverages may be considered upper limits and thus, for the compositions of cirrus clouds explored, we do not expect significant heterogeneous chemistry of methanol, acetone, or acetaldehyde with the possible exception of methanol on supercooled HNO_3/H_2O solution.

Number densities of cirrus clouds are highly variable ranging anywhere from ~20 to 20 000 $\mu m^2/cm^3$. However, because the expected coverages are so small, even the largest surface area clouds will not act as significant sinks for these organic molecules. For example, for a 20 000 $\mu m^2/cm^3$ cloud, only 0.065% of atmospheric methanol would be lost from the gas phase to the cloud. Therefore, cirrus clouds are not likely to act as a significant sink for methanol, acetone, or acetaldehyde.

A recent study of HO_x measurements in the upper troposphere observed a correlation between high values of formaldehyde, CH_2O, and high values of methanol, CH_3OH, in the presence of cirrus clouds.[14] This study introduces the possibility of heterogeneous oxidation of methanol to formaldehyde on the cirrus as an explanation with a required sticking coefficient of methanol on ice of ≥ 0.01. The largest sticking coefficient that we were able to measure at 200 K was on a supercooled HNO_3/H_2O solution, which is still approximately 3 times lower than 0.01. Furthermore, supercooled HNO_3/H_2O solutions are unlikely to form under typical cirrus cloud conditions because high pressures of HNO_3 are required. We also did not observe any gas-phase reaction products. Despite the fact that we do not measure such a large sticking coefficient of methanol on pure ice at cirrus cloud temperatures, we do see an increased reactivity of methanol on a supercooled HNO_3/H_2O solution. The observed increased sticking coefficient could imply that reactivity of methanol on ice in the presence of other species or on aerosols may be large enough for the conversion of methanol to formaldehyde to occur.

Acknowledgement. M.A.T. thanks NSF-ATM9711969 and NASA SA98-0005 for funding this work.

References and Notes

(1) Singh, H. B.; Kanakidou, M.; Crutzen, P. J.; Jacob, D. J. *Nature* **1995**, *378*, 50−54.

(2) Singh, H.; Chen, Y.; Tabazadeh, A.; Fukui, Y.; Bey, I.; Yantosca, R.; Jacob, D.; Arnold, F.; Wohlfrom, K.; Atlas, E.; Flocke, F.; Blake, D.; Blake, N.; Heikes, B.; Snow, J.; Talbot, R.; Gregory, G.; Sachse, G.; Vay, S.; Kondo, Y. *J. Geophys. Res.* **2000**, *105*, 3795−3805.

(3) Arnold, F.; Burger, V.; Droste-Fanke, B.; Grimm, F.; Krieger, A.; Schneider, J.; Stilp, T. *Geophys. Res. Lett.* **1997**, *24*, 3017−3020.

(4) Singh, H.; Chen, Y.; Staudt, A.; Jacob, D.; Blake, D.; Heikes, B.; Snow, D. *Nature* **2001**, *410*, 1078−1081.

(5) Holzinger, R.; Warneke, C.; Hansel, A.; Jordan, A.; Lindinger, W.; Scharffe, D. H.; Schade, G.; Crutzen, P. J. *Geophys. Res. Lett.* **1999**, *26*, 1161−1164.

(6) Muller, J.-F.; Brasseur, G. *J. Geophys. Res.* **1999**, *104*, 1705−1715.

(7) Hauglustaine, D. A.; Ridley, B. A.; Solomon, S.; Hess, P. G.; Madronich, S. *Geophys. Res. Lett.* **1996**, *56*, 2609−2612.

(8) Singh, H. B.; Herlth, D.; Kolyer, R.; Salas, L.; Bradshaw, J. D.; Sandholm, S. T.; Davis, D. D.; Crawford, J.; Kondo, Y.; Koike, M.; Talbot, R.; Gregory, G. L.; Sachse, G. W.; Browell, E.; Blake, D. R.; Rowland, F. S.; Newell, R.; Merrill, J.; Jeikes, B.; Liu, S. C.; Crutzen, P. J.; Kanakidou, M. *J. Geophys. Res.* **1996**, *101*, 1793−1808.

(9) Jaegle, L.; Jacob, D. J.; Wang, Y.; Weinheimer, A. J.; Ridley, B. A.; Campos, T. L.; Sachse, G. W.; Hagen, D. E. *Geophys. Res. Lett.* **1998**, *25*, 1705−1708.

(10) Chatfield, R. B. *Geophys. Res. Lett.* **1994**, *21*, 2705−2708.

(11) Iraci, L. T.; Tolbert, M. A. *J. Geophys. Res.* **1997**, *102*, 16099−16107.

(12) Jayne, J. T.; Worsnop, D. R.; Kolb, C. E.; Swartz, E.; Davidovits, P. *J. Phys. Chem.* **1996**, *100*, 8015−8022.

(13) Crawford, J.; Davis, D.; Olson, J.; Chen, G.; Liu, S.; Fueberg, H.; Hannan, J.; Kondo, Y.; Anderson, B.; Gregory, G.; Sachse, G.; Talbot, R.; Viggiano, A.; Heikes, B.; Snow, J.; Singh, H.; Blake, D. *J. Geophys. Res.* **2000**, *105*, 19795−19809.

(14) Jaegle, L.; Jacob, D. J.; Brune, W. H.; Faloona, I.; Tan, D.; Heikes, B. G.; Kondo, Y.; Sachse, G. W.; Anderson, B.; Gregory, G. L.; Singh, H. B.; Pueschel, R.; Ferry, G.; Blake, D. R.; Shetter, R. E. *J. Geophys. Res.* **2000**, *105*, 3877−3892.

(15) Takano, Y.; Liou, K. N. *J. Atmos. Sci.* **1995**, *8*, 321−330.

(16) Zondlo, M. A.; Barone, S. B.; Tolbert, M. A. *Geophys. Res. Lett.* **1997**, *24*, 1391−1394.

(17) Abbatt, J. P. D. *Geophys. Res. Lett.* **1997**, *24*, 1479−1482.

(18) Golden, D. M.; Spokes, G. N.; Benson, S. W. *Angew. Chem., Int. Ed. Engl.* **1973**, *12*, 534−546.

(19) Greenler, R. G. *J. Chem. Phys.* **1966**, *44*, 310−315.

(20) Barone, S. B.; Zondlo, M. A.; Tolbert, M. A. *J. Phys. Chem. A* **1997**, *101*, 8643−8652.

(21) Hudson, P. K.; Shilling, J. E.; Tolbert, M. A.; Toon, O. B. *J. Geophys. Res.*, submitted for publication, Feb. 2002.

(22) Zondlo, M. A.; Onasch, T. B.; Warshawsky, M. S.; Tolbert, M. A.; Mallick, G.; Arentz, P.; Robinson, M. S. *J. Phys. Chem. B* **1997**, *101*, 10887−10895.

(23) Marti, J.; Mauersberger, K. *Geophys. Res. Lett.* **1993**, *20*, 363−366.

(24) Zondlo, M. A.; Barone, S. B.; Tolbert, M. A. *J. Phys. Chem. A* **1998**, *102*, 5735−5748.

(25) Jayne, J. T.; Duan, S. X.; Davidovits, P.; Worsnop, D. R.; Zahniser, M. S.; Kolb, C. E. *J. Phys. Chem.* **1991**, *95*, 6329−6336.

(26) Donaldson, D. J.; Anderson, D. *J. Phys. Chem. A* **1999**, *103*, 871−876.

(27) Ravishankara, A.; Hanson, D. *J. Geophys. Res.* **1996**, *101*, 3885−3890.

(28) *Handbook of Chemistry and Physics*, 73rd ed.; Lide, D. R., Ed.; CRC Press: Boca Raton, FL, 1992−1993.

(29) *Scientific Assessment of Stratospheric Ozone: 1989*; Global Ozone Research and Monitoring Project: Geneva, 1989; Vol. WMO, Report 20.

(30) Gaffney, J. S.; Senum, G. I. Peroxides, Peracids, Aldehydes, and PANs and Their Links to Natural and Anthropogenic Organic Sources. In *Gas−Liquid Chemistry of Natural Waters*; Newman, L., Ed.; Brookhaven National Laboratory: Upton, NY, 1984; Vol. 1; pp 5-1−5-7.